

Experimental Study of the Unstart/Restart Process of a Two-Dimensional Supersonic Inlet Induced by Backpressure

Y. L. Zhao, Y. Y. Zhou[†] and Y. X. Zhao

Science and Technology on Scramjet Laboratory, College of Aerospace Science and Engineering, National University of Defense Technology, Changsha, Hunan, 410073, People's Republic of China

[†] *Corresponding Author Email: zhouyongyi13@nudt.edu.cn*

(Received July 24, 2021; accepted October 10, 2021)

ABSTRACT

Unstart/restart phenomena induced by backpressure in a general inlet with a freestream of $M = 2.7$ are investigated in an in-draft supersonic quiet wind tunnel. The boundary layers are turbulent on the forebody while are laminar on the lip wall, which could mimic real flight conditions. The high-speed Schlieren imaging system and the nanoparticle-based planar laser scattering (NPLS) method are used to visualize the inlet flowfield. The inlet wall pressure is measured by high-frequency pressure transducers. The backpressure is reproduced by downstream transverse jets other than mechanical throttlers, which is more suitable to mimic backpressure caused by combustion. The high spatio-temporal resolution full-view images of inlet flow features during the complete unstart/restart process are captured, which are seldom seen before. The formation and disappearance process of massive boundary layer separation at the entrance of the unstarted inlet is observed. The backpressure transmits upstream through the shock wave/boundary layer interaction (SWBLI) regions. The shock structures change the angles and merge upstream to balance the pressure rise. The Mach shock reflection configuration is observed in both unstart/restart process, accompanied by the boundary layer separation extending to the leading edge. The experiment also revealed notable hysteresis in the unstart/restart process.

Keywords: Supersonic inlet; Backpressure; Unstart; Shock configuration; Boundary layer separation; Wind tunnel; Flow visualization.

1. INTRODUCTION

The supersonic inlet is an air-intake part of the scramjet engine responsible for capturing, slowing down and compressing the incoming air for downstream combustion (Billig 2008; Balent and Kutschenreuter 1965; Jayakrishnan and Deepu 2021; Senthilkumar and Muruganandam 2020; Zhou and Wang 2019). The inlets must operate in the started mode for proper function. The inlets in an unstarted mode typically capture less air flow and have low air compression efficiency (Wagner *et al.* 2012a; Li *et al.* 2013; John and Senthilkumar 2018), which could be dangerous for the scramjet or even the whole vehicle (Volland *et al.* 2013; Shimura *et al.* 1998; Tan *et al.* 2009; Poggie *et al.* 2015). Inlet unstart issue has attracted much attention by researchers over recent decades. Many factors may lead to inlet unstart, including improper design, boundary layer separation and movement of the shockwave train (Chang *et al.* 2013; Do *et al.* 2011b; Tan *et al.* 2011; Tao *et al.* 2014; Vignesh Ram and Kim 2020). The backpressure caused by downstream fuel combustion is another cause of unstart. The fuel mixture is

affected by pressure oscillations and causes heat release oscillations (Semlitsch *et al.* 2017). In the design state, the downstream combustion backpressure can be held in the isolator. When the heat release is unsteady, the pressure waves could affect the upstream flow (Juniper and Sujith 2018) and make the combustion chamber pressure fluctuate (Shi *et al.* 2019). The certain value backpressure transmits upstream and can lead the inlet to unstart.

Backpressures have been mainly mimicked through mechanical throttles (Flock and Gülhan 2015; Deng *et al.* 2017), thermal choking or heat releases (Im *et al.* 2016) and mass injection (Do *et al.* 2011a). It is effective to investigate the unstart process (Srikant *et al.* 2010; Wagner *et al.* 2012b), even though it would omit flow behaviors influenced by oil injection or heat release. Considering it is challenging to reproduce all backpressure elements, mass injection is a more suitable way to reproduce backpressure rise in practice by contrast (Im and Do 2018). However, few previous researches adopted this method

(Tan *et al.* 2009; Do *et al.* 2011a; Do *et al.* 2011b; Im *et al.* 2016). The inlet unstart process has been a focus of many studies. The process of inlet unstart caused by deflecting a flap at the end of the isolator was investigated (Wagner 2009; Wagner *et al.* 2012a). The shockwave propagation was visualized. It is found that unstart is associated with boundary layer separation. The unstarted inlet flow field was investigated numerically (Su and Zhang 2013) and experimentally (Tan *et al.* 2012). The influence of the boundary layer on inlet unstart was experimentally studied (Do *et al.* 2011a; Do *et al.* 2011b). The results reveal that the characteristics of initial boundary layer strongly affect the unstart dynamics.

Previous research on supersonic inlet backpressure induced unstart focused not only on the characteristics of the unstarted flowfield but also on the flowfield transformation of the unstart/restart process. Chang *et al.* (2009) studied the unstart/restart characteristics of supersonic inlets and reported the causes of unstart/restart phenomena is the formation and disappearance of separation at the entrance. Chang *et al.* (2014) proposed a backpressure unstart detection method based on the history of wall static pressures. Jiao *et al.* (2016) studied two general overall wave configurations in hypersonic inlets. Li *et al.* (2018) investigated the unstart/restart properties in turbine-based combined cycle (TBCC) inlets numerically. They found that the mass flow rate does not change with increasing backpressure for a certain transition stage, and that, once inlet unstart occurs, the mass flow rate decreases rapidly.

In this study, experiments are designed to reveal the unstart/restart process of a supersonic inlet induced by backpressure. The experiments are conducted in a supersonic quiet wind tunnel. The boundary layers developed on the forebody are turbulent and are laminar on the lip wall, which is closer to real flight conditions compared to the previous researches. The backpressure is reproduced by downstream transverse jets. The transformation process of the flowfield in a general two-dimensional inlet is recorded by a high-speed Schlieren photography system and NPLS method. The pressure data along the wall centerline is monitored by pressure transducers. The unstart/restart flowfield and the hysteresis in the unstart/restart process are analyzed.

2. EXPERIMENTAL SETUP

2.1 Wind Tunnel Facility and Test Model

The experiments are conducted in an in-draft supersonic quiet wind tunnel (Fig.1) at the National University of Defense and Technology (Wang *et al.* 2012a; Wang *et al.* 2012b). The flow generated by the wind tunnel is of low turbulence, which is effective to reproduce real flight conditions at high altitude. The test section is $M = 2.7$. The total pressure of the flow is 1 atm (101 kPa) and the total temperature is 300 K. The wind tunnel can work continuously for more than 30 s. The length of the test section is 400 mm, and the cross-section size is 200 mm \times 200 mm. The sidewalls and upper wall of the test section are made of optical glass to facilitate optical observation of the flowfield.

Table 1. Flow conditions of the wind tunnel.

M_∞	$p_0(kPa)$	$T_0(K)$	$p_w(kPa)$	$T_w(K)$	$U_\infty(m/s)$
2.7	101	300	4.3	122.1	597.9

The configuration of a scramjet inlet can be generally summarized as being composed of a compression surface and an internal flow channel (which could be regarded as isolator). The unstart/restart mechanism of the two-dimensional inlets are universal, which means it is suitable for three-dimensional inlets as well (Zhao *et al.* 2014; Wang *et al.* 2015). To facilitate the observation of the flowfield, the experimental model used in the experiments are simplified to a two-dimensional supersonic inlet without forebody compression (Fig. 2). The characteristics of inlet start are determined by internal compression, so the external compression part of the inlet is omitted in the test model. The contraction ratio of the inlet is 1.38. Although forebody compression is not considered in this inlet, a flat forebody is still retained parallel to the incoming flow of the wind tunnel to produce a turbulent boundary layer (Fig. 2). In the internal contraction segment of the inlet, the incoming flow is compressed by the lip of the inlet and the flow direction is deflected. The compression angle of the lip is 8° , so the angle between the internal flow of the inlet and the external flow is 8° . The design of the inlet can be used to investigate the unstart/restart characteristics of the supersonic inlet at $M = 2.7$.

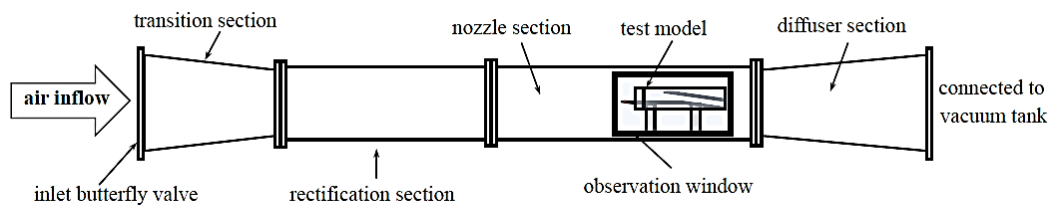


Fig. 1. Sketch of the wind tunnel.

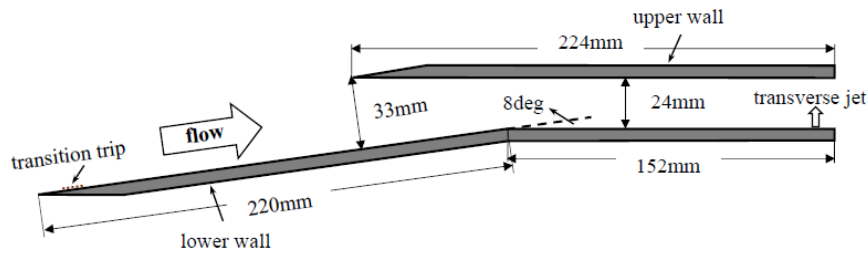


Fig. 2. Side-view sketch of the test model.

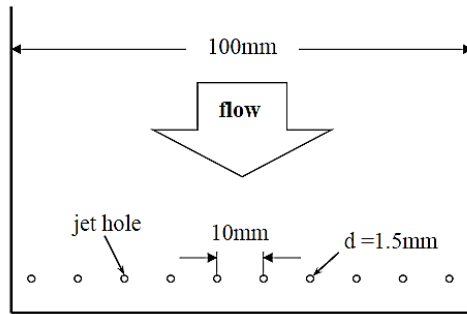


Fig. 3. Overlooking sketch of the test model transverse jet holes.

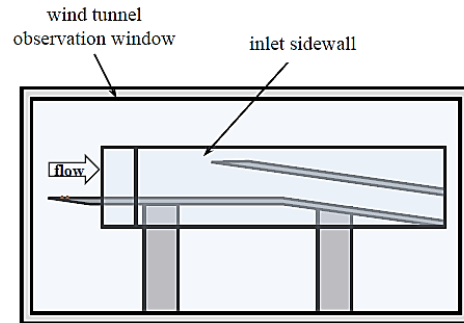


Fig. 4. Side-view sketch of the test model mounted in the wind tunnel.

As the flow of the wind tunnel is low-turbulence and the length of the forebody of the inlet is not sufficient to make the boundary layer turbulent spontaneously, a transition trip is attached to the leading edge. The transition trip is made of sandpaper with a width of 10 mm located 10 mm downstream of the leading edge of the forebody, which can be seen in Fig. 2.

The transverse jets are located near the exit of the inlet (Fig. 2). There are ten jet holes with diameters of 1.5 mm equally spaced on the lower wall of the inlet constituting a transverse jet array. The transverse jets are used to generate backpressure to induce inlet unstart. There is a common jet supply chamber linked with all the jet holes in the lower wall. The chamber is a cylinder with a diameter of 10 mm. A schematic of the transverse jets array is shown in Fig. 3.

The test model installed in the test section of the wind tunnel is shown in Fig. 4. The width of the inlet is 100 mm. As the width of the wind tunnel test section is 200 mm, in order to prevent side spillage of the inlet flow, sidewalls with height of 80 mm are installed on both sides of the inlet. The sidewalls and the upper wall of the inlet model are made of optical glass so that the whole flowfield of the inlet could be observed. The thickness of the optical glass is 10 mm. The bottom wall of the inlet is made of carbon steel.

2.2 Flow Visualization Technology and Pressure Measurements

The high-speed Schlieren photography system is used in experiments to investigate the dynamic flowfield. The size of the Schlieren system is 200 mm in diameter. A tungsten lamp is used as the light

source of the Schlieren system. The images are acquired using a high-speed camera. The shutter time of the camera is 1/3015 second, and the image acquisition frequency is 3000 fps, which is sufficient for capturing dynamic changes of the flowfield in the unstart/restart process of the inlet. The standard Z-shaped optical path of the Schlieren system is adopted in the experiments. The optical path is deflected by two concave mirrors with diameters of 200 mm before and after the test section. The reflection angles of the two mirrors are arranged as closely parallel as possible.

The nanoparticle-based planar laser scattering (NPLS) experimental method developed by Zhao *et al.* (2009) is employed for fine flow visualization. The nanoparticle used as a tracer particle in present investigation is TiO_2 . To illuminate the seeded flow, a dual cavity Nd:YAG 532 nm laser system developed by BeamTech is used. The laser system with 520 mJ maximum pulse energy output could provide a stable, high-energy and uniform light sheet, whose width and thickness are about 200 mm and 0.2 mm respectively. Two 8-bit IMPERX charge-coupled device (CCD) cameras with resolution of 4096×2600 pixels are arranged side by side to capture two images with partial repetition at the exact same moment. The two images could be merged to enlarge the vision scale without reducing the resolution. The cameras are equipped with Sigma Macro 105 mm f/2.8D lens. The f number is set to 2.8 during the experiment. A synchronizer is employed to synchronize the CCD cameras and the laser system.

The inlet pressure signals are measured through pressure transducers (Shanghai Tianmu Automation,

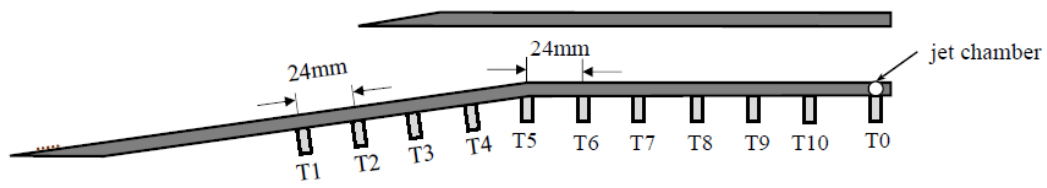


Fig. 5. Arrangement of the pressure transducers mounted under the test model.

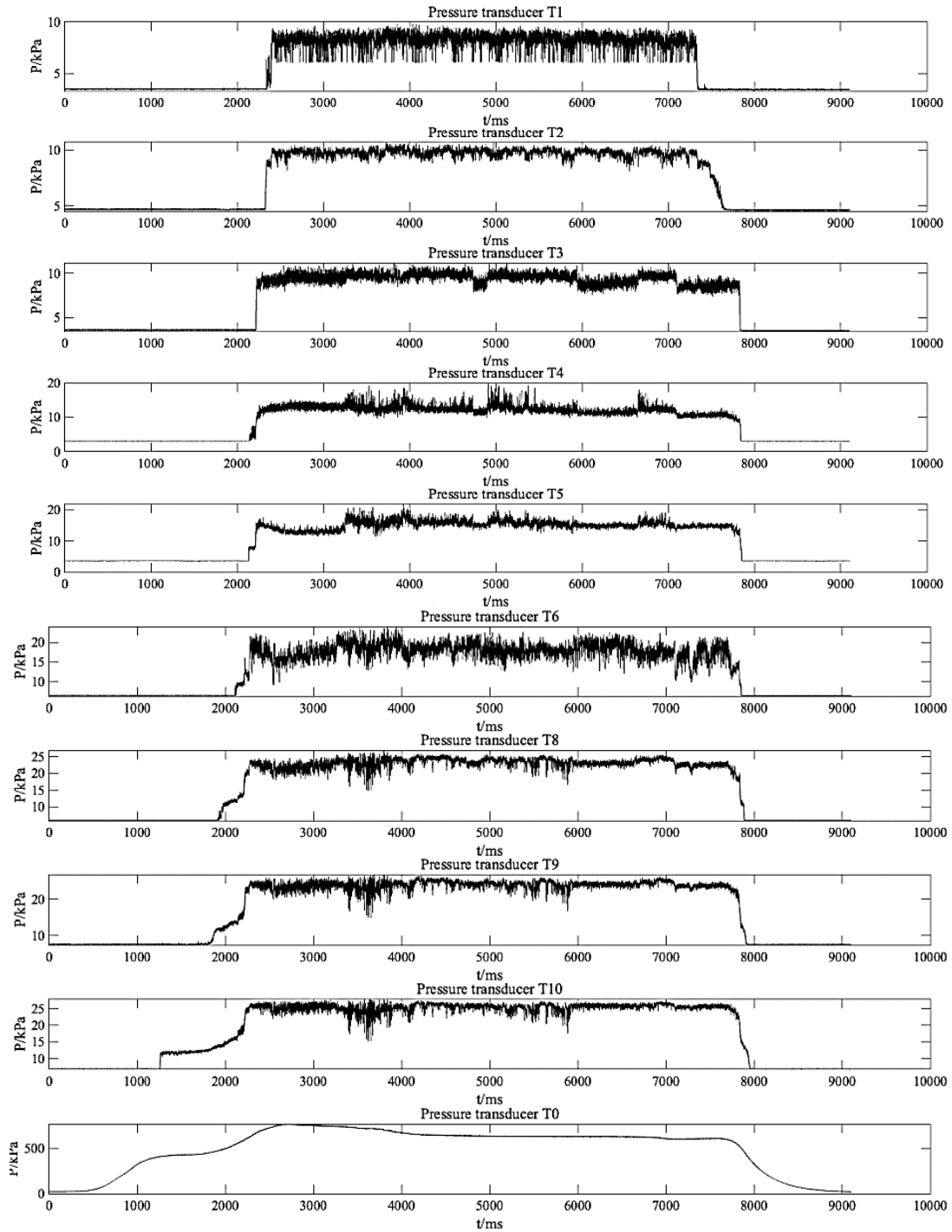


Fig. 6. Static pressure history during a run.

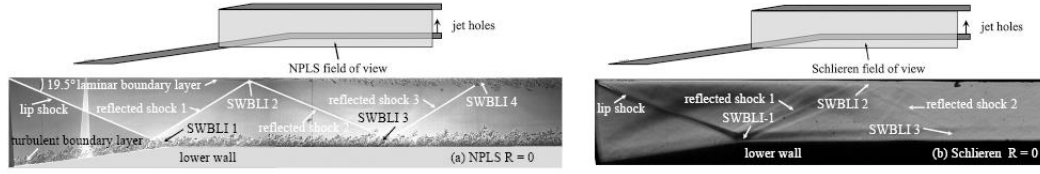


Fig. 7. NPLS and Schlieren images of the flowfield of the started inlet (a) NPLS image (b) Schlieren image.

Inc.) mounted along the centerline on the lower wall, which are shown in Fig. 5. The T5 transducer is mounted at the shoulder of the inlet under the lower wall. The distance between two adjacent pressure transducers is 24 mm. The jet chamber pressure is monitored by transducer T0. Testing range and precision of the transducers T1-T10 are 0-100 kPa and 0.2 kPa respectively. Testing range and precision of the transducer T0 are 0-1 MPa and 2 kPa respectively. The response frequency of the pressure transducers is up to 20 kHz. Pressure signals are acquired through data acquisition system (Wuhan Patrontest Ltd.) with a sampling rate of 10 kHz.

3. RESULTS AND ANALYSIS

In the experiments, the valve of the transverse jets is opened manually after the inlet start. Under the action of the transverse jets, backpressure in the inlet is induced. The transverse jet intensity is gradually increased until inlet unstart. The flowfield transformation in the unstart process is recorded. After the inlet unstart, the transverse jet intensity is then decreased, and the flowfield transformation in the restart process is recorded. Gas chamber pressure is measured by T0 in real time. The pressure data history of T1-T10 and the jet chamber during a run are shown in Fig. 6. The pressure transducer T7 does not work during the experiment, so the pressure data at the exact location is not shown.

Considering the pressure ratio of the jet and the inlet flow and the diameter of the jet hole, the transverse jet in this study could be regarded as sonic. To evaluate the strength of jet caused backpressure increase, the momentum flux ratio of the jet to that of the freestream is adopted, which is defined by:

$$R = \frac{\sqrt{(\rho u^2)_{jet}}}{\sqrt{(\rho u^2)_{\infty}}} = \frac{\sqrt{(\gamma p M^2)_{jet}}}{\sqrt{(\gamma p M^2)_{\infty}}} \quad (1)$$

Here, ρ , u , γ , p and M are gas density, velocity ratio of specific heats, pressure, and Mach number of the jets (subscript *jet*) and freestream (subscript ∞). The ratio of specific heats is $\gamma = 1.4$.

3.1. Analysis of the Started Flowfield

In the experiments, the wind tunnel is opened first and the flowfield of the wind tunnel is subsequently established. As the contraction ratio of the inlet is relatively low, the Mach number of the wind tunnel is high enough for the inlet to start without the transverse jets operating. To facilitate observation,

NPLS and Schlieren images are taken with a counterclockwise rotation of 8° to make the internal flowfield of the inlet horizontal. The NPLS and Schlieren images of the flowfield of the started inlet could be seen in Fig. 7.

Some angles should be defined in advance. The lip shock angle in the figure is defined as $\beta_{lip_{rotated}}$, and the shock angle measured by freestream direction is defined as β_{ls} . The relationship between the two angles is $\beta_{ls} = \beta_{lip_{rotated}} + 8^\circ$. The deflection angle is defined as θ . In the following figures, SWBLL indicates shockwave/boundary layer interaction. Owing to the low-turbulence quality of the incoming flow and the smoothness of the model upper wall, the boundary layer is still laminar at the SWBLL 2 region (could be seen in Fig. 7 (a)). Under the action of the transition trip ahead of the lower wall, the flow turns turbulent at SWBLL 1 region. The lip shock angle is $\beta_{lip_{rotated}} = 19.5^\circ$, with the rotation angle removed, and the flow Mach number after lip shock is 2.34 according to the oblique shockwave relationship. The lip shock first impinges on the inlet lower wall near the shoulder (could be known from the pressure distribution). As the flow expands at the shoulder, the expansion waves intersect with the incident lip shock, the intensity of the lip shock is weakened, and there is no obvious separation in the turbulent boundary layer. The lip shock is reflected by the lower wall and then impinges on the inlet upper wall. The laminar boundary layer separates slightly under the adverse pressure gradient caused by the incident shockwave, which implies that the laminar boundary layer separates much more easily than turbulent boundary layer. The lip shock is then reflected by the inlet upper wall and impinged on the inlet lower wall again. The reflection shock 3 and the SWBLL 4 region could be recognized in the NPLS image.

3.2 Analysis of the Unstart Process

Based on the analysis of the started flowfield of the inlet, the flowfield transformation in the backpressure-induced unstart process of the inlet is investigated first. The NPLS images of the flowfield in the inlet unstart process are shown in Fig. 8, and the Schlieren images are shown in Fig. 9. The respective images correspond to different backpressure intensities.

As shown in Fig. 8(c), the separation shock induced by the transverse jets impinges on the lower wall of the inlet at $R = 3.967$. With the adverse pressure gradient induced by the separation shock 5, the boundary layer on the upper wall separates at the

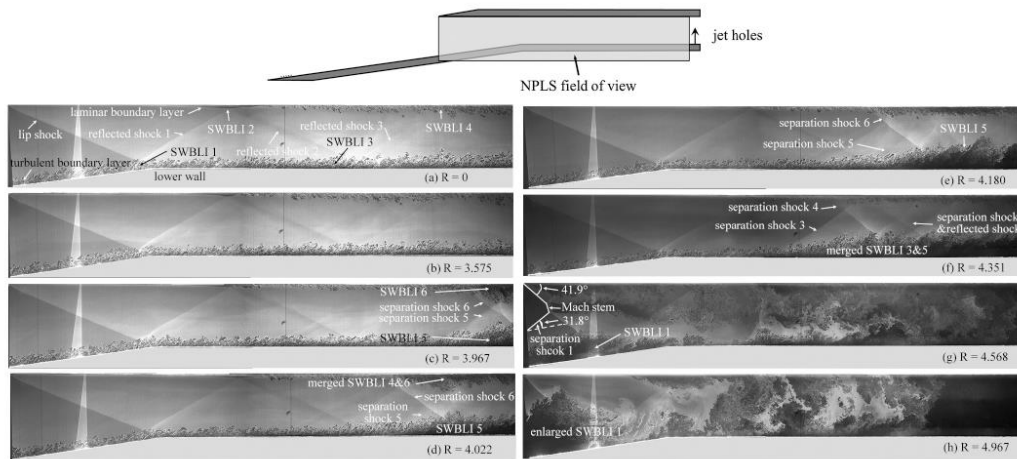


Fig. 8. NPLS images of the inlet unstart process.

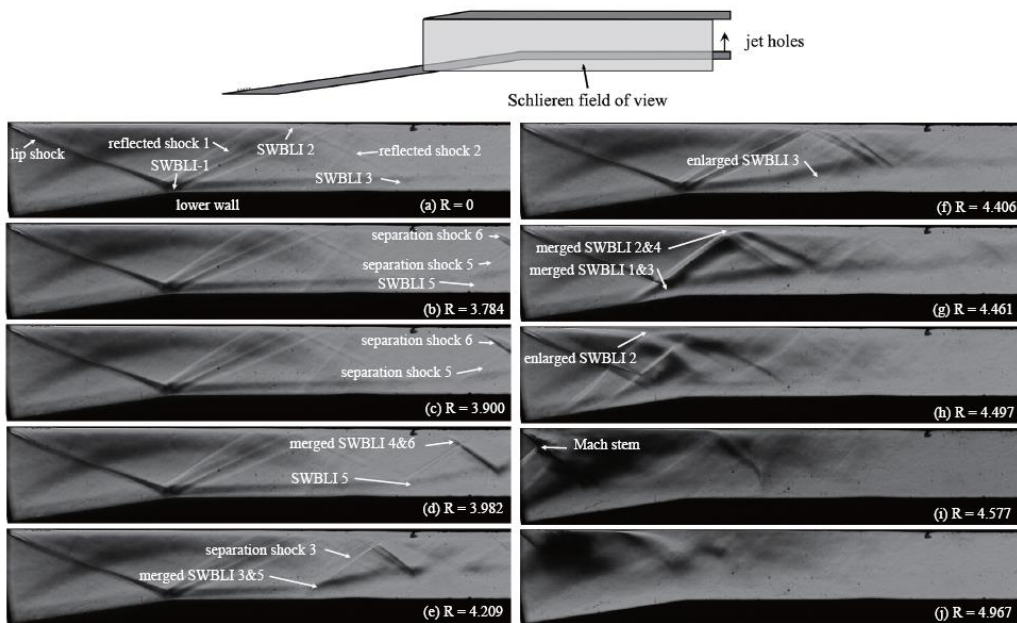


Fig. 9. Schlieren images of the inlet unstart process.

impingement location, forming the SWBLI 6 region and the separation shock 6. With the jet intensity increasing, the inlet backpressure continues to increase, causing the SWBLI 5 region on the lower wall to increase gradually (Fig. 9(d)). The separation shock 5 moves upstream with the enlargement of the SWBLI 5 region. At $R = 4.022$ (Fig. 8(d)), the SWBLI 6 region induced by the separation shock 5 merges with the SWBLI 4 region induced by the reflected shock 3. The first separation region mergence occurs. The separation shock 6 moves upstream with the SWBLI 5 region growing (Fig. 8(e)). From $R = 4.209$ to $R = 4.351$ (Fig. 9(e) and Fig. 8(f)), the SWBLI 5 region blends with the SWBLI 3 region. The second separation region mergence occurs. The separation shock induced by the separation region and its reflected shock forms the complicated shock structures in the inlet. With the

SWBLI 3 region growing, the separation shock 3 moves upstream. The reflected shock 2 could not match the pressure rise, so it is swallowed by the separation shock 3. The mergence of SWBLI 2 and 4 regions on the upper wall and the mergence of SWBLI 1 and 3 regions on the lower wall almost happen at the same time (Fig. 9(g)). The laminar boundary layer on the upper wall has less ability to resist the adverse pressure, so the SWBLI 2 enlarges rapidly with the backpressure rising (Fig. 9(h)). The SWBLI 1 region forms a large-scale separation region, and the separation shock is pushed out of the inlet lip, which indicates the inlet unstart.

The time-averaged static pressure, scaled by the freestream static pressure, along the lower wall in the unstart process is shown in Fig.10. The error bars donate the standard deviation. The pressure distribution at $R = 0$ indicates that the lip shock

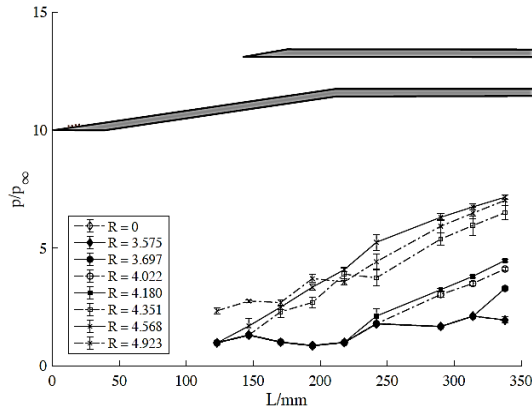


Fig. 10. Time-averaged static pressure along the lower wall in the unstart process. The error bars donate standard deviation.

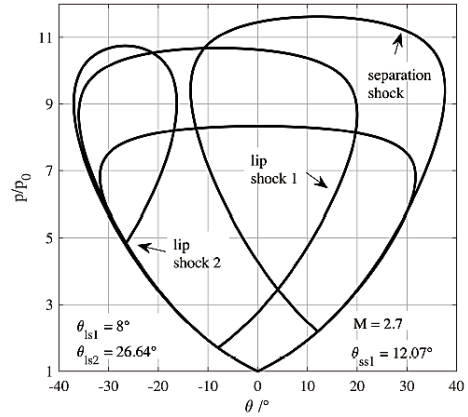


Fig. 11. Shock polar when lip deflection angle θ_{ls} increases at $M = 2.7$.

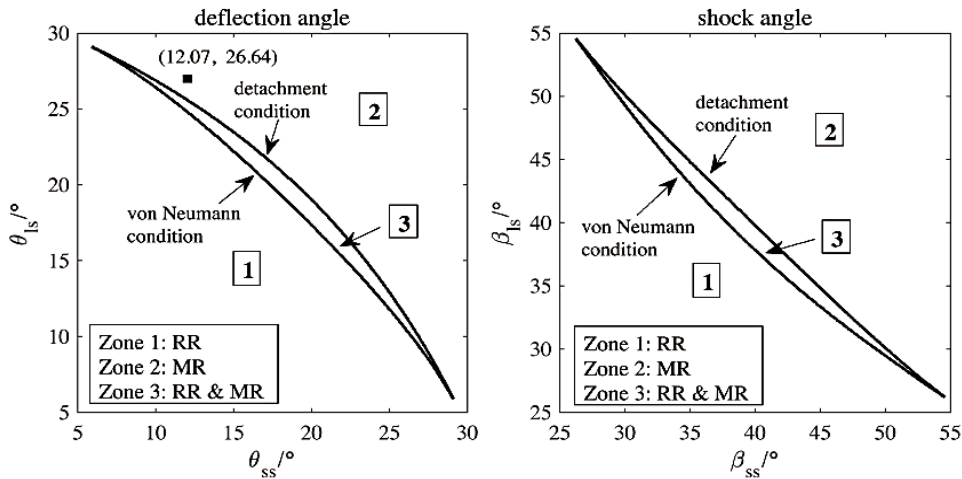


Fig. 12. Relationship between lip deflection/shock angle and separation deflection/shock angle at $M = 2.7$.

impinges a little downstream of the shoulder, because the pressure rises at T6. With the jet intensity rising, the static pressure increases gradually. The backpressure spreads upstream through the separation region, so the unseparated boundary layer does not have an apparent pressure rise. The mainstream and the shock could balance the resistance caused by rising pressure.

In Fig. 8(g), the SWBLI 2 separation region extended to the lip leading edge could be investigated (Tao *et al.* 2016; Tao *et al.* 2017). Moreover, the Mach reflection wave configuration flowfield at the inlet lip could also be investigated in Fig. 8 (g) and Fig. 9(i). In Fig. 9 (h), when $R = 4.497$, the lip shock angle attached to the upper wall is $\beta_{liprotated} = 19.5^\circ$, which means $\beta_{ls} = 27.5^\circ$. The SWBLI 2 region is not enlarged yet. In Fig. 8(g), when $R = 4.568$, the lip shock angle attached to the upper wall is $\beta_{liprotated} = 41.9^\circ$, which indicates the shock angle measured by freestream direction is $\beta_{ls2} = 49.9^\circ$. The separation shock angle attached to the lower wall is $\beta_{ss1} = 31.8^\circ$. Figure 11 gives shock polar under $M = 2.7$ to illustrate the solutions of reflection configuration.

The shock polar indicates that the Mach reflection configuration is unique (Tao *et al.* 2014). The deflection angles are $\theta_{ls1} = 8^\circ$, $\theta_{ls1} = 12.07^\circ$ and $\theta_{ss1} = 26.64^\circ$, corresponding to lip shock 1 (without large separation), lip shock 2 (with large separation) and lower wall separation shock respectively.

The phenomena reflect that this flowfield state is steady during the unstart process of the inlet. Two factors that contribute to the Mach reflection and boundary layer separation extending to the leading edge are considered. One factor is the lower wall separation shock angle, and the other one is the shock impingement point on the upper wall. Figure 12 shows the relationship between shock wave configuration and separation deflection/shock angle and lip deflection/shock angle. The three zones are divided by two curves plotted according to von Neumann condition and detachment condition (Ben-Dor 2013). The lip shock and separation shock could only be regular reflection in zone 1 and Mach reflection in zone 3. The zone 2 is the dual solution zone, where the shock configuration could be regular reflection or Mach reflection. When $R = 4.497$, the

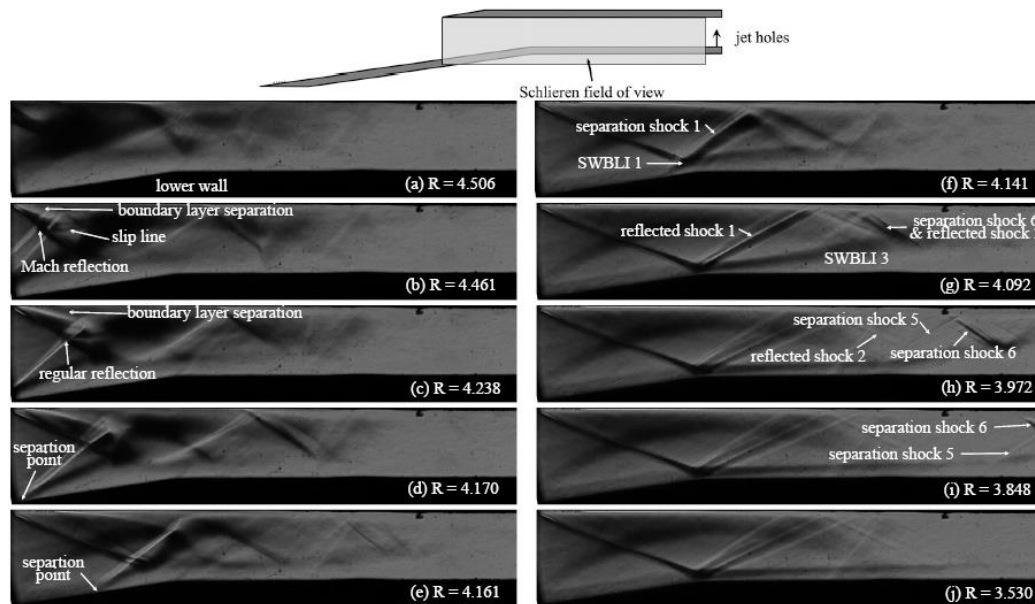


Fig. 13. Schlieren images of the inlet restart process.

separation shock angle is small, and the wave configuration is regular reflection. The lip shock remains $\beta_{ls} = 27.5^\circ$ until $R = 4.568$. The separation angle is far smaller than 31.8° , so the shock configuration is regular reflection. According to the free-interaction theory, the rising backpressure makes the separation region on the lower wall enlarge, the separation point move upstream and the separation shock angle increase. As a result, the separation shock impingement point on the upper wall moves upstream. Meanwhile, the strength of the lip shock could not provide enough pressure rise to balance the high pressure in SWBLI 2 region, so the lip shock is merged by the separation shock on the upper wall. The lip shock angle increases as well. Restricted by the lip leading edge, the separation region could not move upstream under the action of backpressure. The lip shock (still is oblique shock) continues to increase to balance the pressure rise. Finally, the lip shock and separation shock form the status marked by a black square in Fig.12 in zone 2. When Mach reflection occurs, even the inlet is still started, the total pressure loss after the Mach stem is severe, which should be avoided in engineering application.

3.3. Analysis of the Restart Process

Figure 13 and Fig.14 respectively show the Schlieren and NPLS images of the inlet flowfield during the restart process. After the inlet unstart, the jet intensity is reduced gradually. Till the jet intensity is $R = 4.506$, the massive separation regions are at the inlet entrance (Fig. 13(a)). With the jet intensity dropping, the separation regions shrink. It makes the inflow deflection angle smaller and the separation shocks intersect at the internal inlet. The boundary layer separation extending the leading edge could also be investigated in Fig. 13(b) and (c). The shock wave configuration changes with the separation angle changing. With the jet intensity decreasing, both

upper wall and lower wall separation regions shrink, the shock angles turn wall-towards, and the Mach reflection configuration (Fig.13(b)) turns to regular reflection configuration (Fig.13(c)). In Fig. 13(b), the slip line downstream of the Mach stem could be seen.

When the jet intensity is among $R = 4.170$ and $R = 4.141$, the SWBLI 1 and 2 regions attach to the wall. The separation point moves downstream to the shoulder in Fig. 13(d) to (f). The turbulent boundary layer separation region on the lower wall turns small step by step along with the drop of the backpressure. The laminar boundary layer separation region on the upper wall turns more rapidly than that of the boundary layer separation region. The lip shock establishes when $R = 4.141$ and reflected shock 1 establishes when $R = 4.092$. The reflected shock 2 and separation shock 6 exist at the same time. With the decrease of the backpressure, the downstream separation regions become smaller, and the separation shocks move downstream (seen in Fig. 13(i)-(j) and Fig. 14(e)-(h)), until all the separation shocks disappear. When the jet intensity is $R = 2.363$, the inlet has restarted totally. In the whole restart process, the SWBLI regions on the both upper wall and lower wall almost reappear in the meantime, which is different from that in the unstart process. The time-averaged static pressure along the lower wall in the restart process is shown in Fig.15. The pressure decreases back to the started condition gradually from upstream to downstream, when the backpressure drops.

3.4. Hysteresis in the Unstart/Restart Process

The NPLS images of the inlet unstart/restart process are shown in Fig.16. Under the same jet intensity, the inlet flowfield is different during the unstart process and the restart process. The discrepancy of the

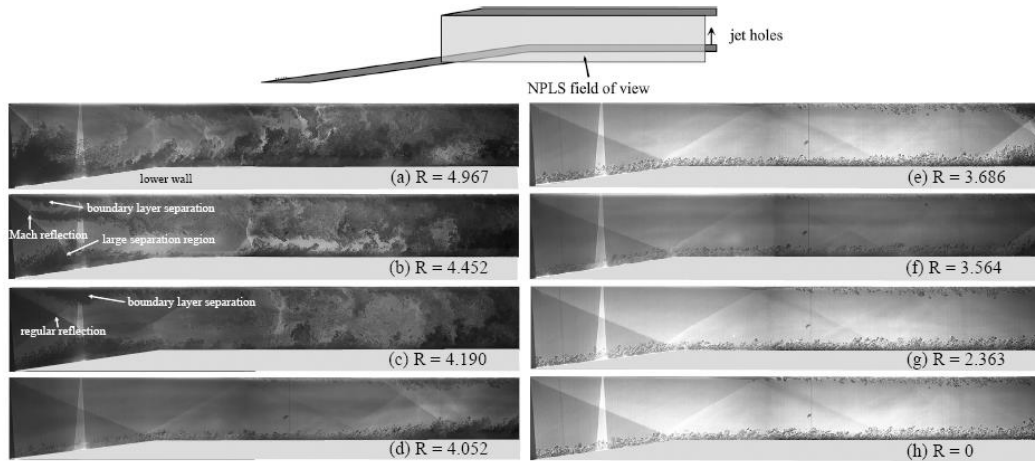


Fig. 14. NPLS images of the inlet restart process.

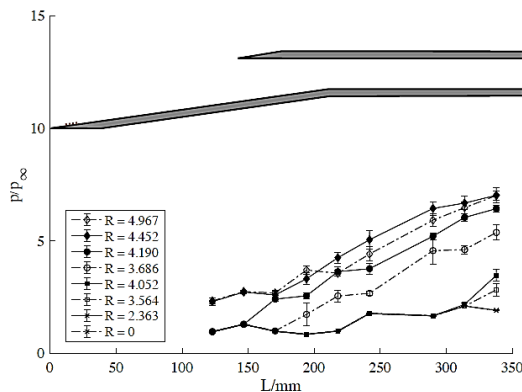


Fig. 15. Time-averaged static pressure along the lower wall in the restart process. The error bars donate standard deviation.

flowfield means that there is a significant hysteresis between the unstart and restart process of the inlet.

Figures 16(a)-(h) show the flowfield in the inlet unstart process and Fig. 16(i)-(p) show the restart process. When the jet intensity rises from $R = 3.575$ to $R = 3.697$ during the unstart process, the downstream separation shocks move upstream, apparently. However, when the jet intensity falls from $R=3.686$ to $R=3.564$, the separation shocks move slower. Near the end of the unstart process, when the jet intensity rises from $R = 4.022$ to $R = 4.180$, the downstream separation regions have not dominated the inlet. However, during the restart process, the upstream separation regions are still large when $R = 4.190$. From wall pressure data in Fig.10 and Fig.15, it could also be seen the hysteresis in the unstart/restart process. Under the similar jet intensity, $R = 4.180$ in the unstart process and $R = 4.190$ in the restart process, the pressure distribution is different. However, the same flowfield in different processes have the similar pressure distribution. It means that the hysteresis happens not on the backpressure differing in the unstart and restart process, but on the jet influencing differently on the flowfield in the unstart and restart process. The

relationship between inlet flowfield state and jet intensity R could be briefly summarized. In the unstart process, the higher jet intensity is, the faster the flow field changes. In the restart process, the lower jet intensity is, the faster the flow field changes.

The hysteresis in the unstart/restart process could be explained by the dual solution of the shock reflection at the inlet entrance. In Fig.12, the black square reflects the Mach reflection of the lip shock and separation shock. When the backpressure drops, the tendency of the lip shock and separation shock status marked in the figure should go left-down wise. The status of the shock configuration goes through the Mach reflection zone, the dual solution zone and regular reflection zone successively. The black square is a little beyond dual solution zone, so the shock status goes through zone 2 soon when the backpressure drops. The shock configuration in dual solution is related to the history. As a result, the hysteresis in the unstart/restart process happens.

4. CONCLUSIONS

The backpressure-induced unstart/restart process of the supersonic inlet is investigated experimentally in this study. The inlet backpressure is reproduced by downstream transverse jets. The experiments are conducted in a supersonic wind tunnel at $M = 2.7$. The boundary layers are turbulent on the forebody and laminar on the lip wall mimicking real flight conditions. The whole flowfield transformation in the unstart/restart process of the inlet is recorded by a Schlieren/high-speed photography system and NPLS method. The wall pressure is monitored by pressure transducers. Based on the experimental results, the following conclusions can be drawn.

In the started flowfield of the inlet without backpressure, the lip shock is constantly reflected in the inlet inner flow. The boundary layer on the inlet upper wall is laminar, which separates at the impingement location of the lip shock, and then transition occurs. The boundary layer on the inlet lower wall, having transitioned to turbulent, remains

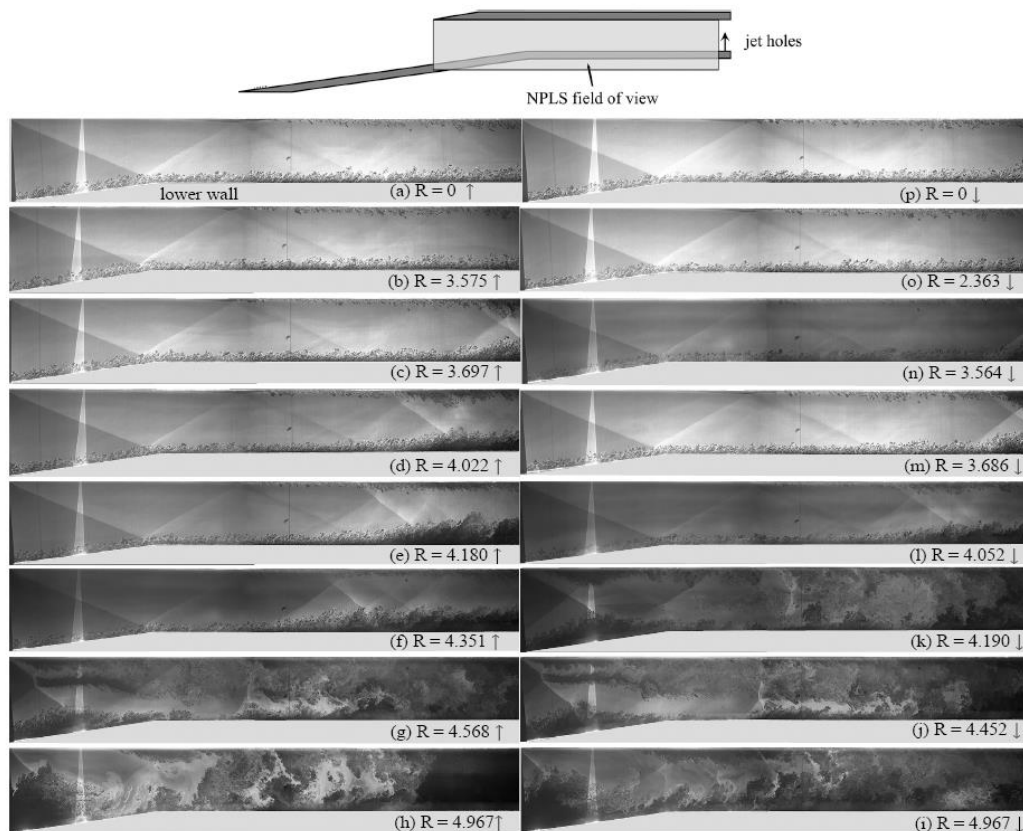


Fig. 16. NPLS images of the inlet unstart/restart process.

attached under the adverse pressure gradient caused by the lip shock. The results prove that boundary layer transition in the inlet flow can restrain boundary layer separation.

In the unstart process of the inlet caused by the increase of the backpressure, the backpressure is transmitted upstream gradually through the boundary layer separation regions, thus affecting the whole isolator. The backpressure affects the size of the separation regions and the position of the separation point, then affects the angle of the shocks. The Mach reflection shock wave configuration could occur in both unstart and restart process, which should be avoided in engineering. The separation shock angle and the impingement point on the upper wall jointly lead to the boundary layer separation extending to the leading edge. In the whole restart process, the SWBLI regions on the both upper wall and lower wall almost reappear in the meantime, which is different from that in the unstart process.

Hysteresis exists in the unstart/restart process of the inlet. The inlet flowfield in the restart process differs greatly from that in the unstart process at the same jet intensity. The difference diminishes as the supersonic flow gradually dominates the inlet. The hysteresis happens not on the backpressure differing in the unstart and restart process, but on the jet influencing differently on the flow field in the unstart and restart process. In the unstart process, the higher jet intensity is, the faster the flow field changes. In the restart process, the lower jet intensity is, the faster

the flow field changes. The dual solution of the lip/separation shock configuration also contributes to the hysteresis.

ACKNOWLEDGMENTS

This work is supported by the National Natural Science Foundation of China (Grant No. 11502294). The authors declare that there is no conflict of interest regarding the publication of this paper.

REFERENCES

- Balent, R. L. and P. H. Kutschenreuter (1965). Hypersonic inlet performance from direct force measurements. *Journal of Spacecraft and Rockets* 2(2), 192–199.
- Ben-Dor, G. (2013). *Shock Wave Reflection Phenomena*. Springer Berlin Heidelberg.
- Billig, F. S. (2008). Supersonic combustion ramjet missile. *Journal of Propulsion and Power* 11(6), 1139–1146.
- Chang, J., L. Wang, W. Bao, J. Qin, J. Niu and W. Xue (2013). Novel Oscillatory Patterns of Hypersonic Inlet Buzz. *Journal of Propulsion and Power* 28(6), 1214–1221.
- Chang, J., D. Yu, W. Bao, Y. Fan and Y. Shen (2009). Effects of boundary-layers bleeding on unstart/restart characteristics of hypersonic

- inlets. *Aeronautical Journal* 113(1143), 319–327.
- Chang, J., R. Zheng, L. Wang, W. Bao and D. Yu (2014). Backpressure unstart detection for a scramjet inlet based on information fusion. *Acta Astronautica* 95(1), 1–14.
- Deng, R., Y. Jin and H. D. Kim (2017). Numerical simulation of the unstart process of dual-mode scramjet. *International Journal of Heat and Mass Transfer* 105, 394–400.
- Do, H., S. K. Im, M. G. Mungal and M. A. Cappelli (2011a). The influence of boundary layers on supersonic inlet flow unstart induced by mass injection. *Experiments in Fluids* 51(3), 679–691.
- Do, H., S. K. Im, M. G. Mungal and M. A. Cappelli (2011b). Visualizing supersonic inlet duct unstart using planar laser Rayleigh scattering. *Experiments in Fluids* 50(6), 1651–1657.
- Flock, A. K. and A. Gülhan (2015). Experimental Investigation of the Starting Behavior of a Three-Dimensional Scramjet Intake. *AIAA Journal* 53(9), 2686–2693.
- Im, S., D. Baccarella, B. McGann, Q. Liu, L. Wermer and H. Do (2016). Unstart phenomena induced by mass addition and heat release in a model scramjet. *Journal of Fluid Mechanics* 797, 604–629.
- Im, S. K. and H. Do (2018). Unstart phenomena induced by flow choking in scramjet inlet/isolators. *Progress in Aerospace Sciences* 97, 1–21.
- Jayakrishnan, S. and M. Deepu (2021). Reacting Flow Simulations of a Dual Throat-Dual Fuel Thruster. *Journal of Applied Fluid Mechanics* 14(01).
- Jiao, X., J. Chang, Z. Wang and D. Yu (2016). Hysteresis phenomenon of hypersonic inlet at high Mach number. *Acta Astronautica* 128(Nov), 657–668.
- John, B. and P. Senthilkumar (2018). Alterations of Cowl Lip for the Improvement of Supersonic-Intake Performance. *Journal of Applied Fluid Mechanics* 11(1), 31–41.
- Juniper, M. P. and R. Sujith (2018, January). Sensitivity and Nonlinearity of Thermoacoustic Oscillations. *Annual Review of Fluid Mechanics* 50(1), 661–689.
- Li, N., J. Chang, C. Jiang, D. Yu, W. Bao, Y. Song and X. Jiao (2018). Unstart/restart hysteresis characteristics analysis of an over-under TBCC inlet caused by backpressure and splitter. *Aerospace Science and Technology* 72, 418–425.
- Li, Z., W. Gao, H. Jiang and J. Yang (2013). Unsteady Behaviors of a Hypersonic Inlet Caused by Throttling in Shock Tunnel. *AIAA Journal* 51(10), 2485–2492.
- Poggie, J., N. J. Bisek, R. L. Kimmel and S. A. Stanfield (2015, January). Spectral Characteristics of Separation Shock Unsteadiness. *AIAA Journal* 53(1), 200–214.
- Semlitsch, B., A. Orchini, A. P. Dowling and M. P. Juniper (2017, December). G-equation modelling of thermoacoustic oscillations of partially premixed flames. *International Journal of Spray and Combustion Dynamics* 9(4), 260–276.
- Senthilkumar, P. and T. M. Muruganandam (2020). Numerical Simulation of Supersonic Flow through Scramjet Intake with Concavity in Cowl Surface. *Journal of Applied Fluid Mechanics* 13(05).
- Shi, W., J. Chang, J. Zhang, J. Ma, Z. Wang and W. Bao (2019, April). Numerical investigation on the forced oscillation of shock train in hypersonic inlet with translating cowl. *Aerospace Science and Technology* 87, 311–322.
- Shimura, T., T. Mitani, N. Sakuranaka and M. Izumikawa (1998, May). Load Oscillations Caused by Unstart of Hypersonic Wind Tunnels and Engines. *Journal of Propulsion and Power* 14(3), 348–353.
- Srikant, S., J. L. Wagner, A. Valdivia, M. R. Akella and N. Clemens (2010). Unstart Detection in a Simplified-Geometry Hypersonic Inlet-Isolator Flow. *Journal of Propulsion and Power* 26(5), 1059–1071.
- Su, W. Y. and K. Y. Zhang (2013). BackPressure Effects on the Hypersonic Inlet-Isolator Pseudoshock Motions. *Journal of Propulsion and Power* 29(6), 1391–1399.
- Tan, H. J., L. G. Li, Y. F. Wen and Q. F. Zhang (2011). Experimental Investigation of the Unstart Process of a Generic Hypersonic Inlet. *AIAA Journal* 49(2), 279–288.
- Tan, H. J., S. Sun and H. X. Huang (2012). Behavior of shock trains in a hypersonic inlet/isolator model with complex background waves. *Experiments in Fluids* 53(6), 1647–1661.
- Tan, H. J., S. Sun and Z. L. Yin (2009, January). Oscillatory Flows of Rectangular Hypersonic Inlet Unstart Caused by Downstream Mass-Flow Choking. *Journal of Propulsion and Power* 25(1), 138–147.
- Tao, Y., X. Fan and Y. Zhao (2014). Viscous effects of shock reflection hysteresis in steady supersonic flows. *Journal of Fluid Mechanics* 759, 134–148.
- Tao, Y., W. Liu and X. Fan (2017, May). Flow visualization for shock-induced boundary layer separation extended to the flat-plate leading edge. *Journal of Visualization* 20(2), 231–235.
- Tao, Y., W. D. Liu and X. Q. Fan (2016). Investigation of shock-induced boundary layer separation extended to the flat plate leading edge. *Acta Mechanica* 227(6), 1791–1797.

- Vignesh Ram, P. S. and T. H. Kim (2020). Numerical Study on Shock Train Characteristics in Divergent Channels. *Journal of Applied Fluid Mechanics* 13(4), 1081–1092.
- Voland, R., A. Auslender, M. Smart, A. Roudakov, V. Semenov and V. Kopchenov (2013). CIAM/NASA Mach 6.5 scramjet flight and ground test. In *9th International Space Planes and Hypersonic Systems and Technologies Conference*, Number c, Norfolk, VA, pp. 1–9. AIAA.
- Wagner, J., A. Valdivia, K. Yuceil, N. Clemens and D. Dolling (2012a). An Experimental Investigation of Supersonic Inlet Unstart. *37th AIAA Fluid Dynamics Conference and Exhibit* (June), 1–20.
- Wagner, J., K. Yuceil, A. Valdivia, N. Clemens and D. Dolling (2012b). PIV Measurements of the Unstart Process in a Supersonic Inlet/Isolator. *38th Fluid Dynamics Conference and Exhibit* (June), 1–21.
- Wagner, J. L. (2009). *Experimental Studies of Unstart Dynamics in Inlet / Isolator Configurations in a Mach 5 Flow*. Ph. D. thesis, the The University of Texas at Austin, Texas, U.S.A.
- Wang, B., W. Liu, Y. Zhao, X. Fan and C. Wang (2012). Experimental investigation of the micro-ramp based shock wave and turbulent boundary layer interaction control. *Physics of Fluids* 24(5), 1166–1175.
- Wang, D., Y. Zhao, Z. Xia, Q. Wang and L. Huang (2012). Experimental investigation of supersonic flow over a hemisphere. *Chinese Science Bulletin* 57(15), 1765–1771.
- Wang, Z., Y. Zhao, Y. Zhao and X. Fan (2015). Prediction of Massive Separation of Unstarted Inlet via Free-Interaction Theory. *AIAA Journal* 53(4), 1108–1112.
- Zhao, Y., Z. Wang, Y. Zhao and X. Fan (2014). Visualization of massive separation of unstarted inlet. *Journal of Visualization* 17(4), 299–302.
- Zhao, Y., S. Yi, L. Tian and Z. Cheng (2009). Supersonic flow imaging via nanoparticles. *Science in China, Series E: Technological Sciences* 52(12), 3640–3648.
- Zhou, L. and Z. Wang (2019). Numerical Investigation on the three-Dimensional Flowfield in the Single Expansion Ramp Nozzle with Passive Cavity Flow Control. *Journal of Applied Fluid Mechanics* 12(4), 1115–1126.